

Seismic-scale geometries and sequence-stratigraphic architecture of Early Cretaceous syn-post rift carbonate systems, Presalt Section, Brazil



M. Minzoni^{1,2*}, A. Cantelli³, J. Thornton³ and B. Wignall³

¹Department of Geological Sciences, University of Alabama, Tuscaloosa, AL 35487, USA

²Work carried out at: Shell International Exploration & Production, Houston, Texas, USA

³Shell Brasil Petróleo Ltda, Rio de Janeiro, Brazil

MM, 0000-0002-9649-1590; AC, 0000-0002-0311-480X; BW, 0000-0003-1731-0876

*Correspondence: mminzoni@ua.edu

Abstract: Regional and detailed seismic stratigraphic analyses of Early Cretaceous (Aptian) presalt carbonate sections from offshore Brazil reveal the complex stratigraphic architecture of late- and post-rift lacustrine carbonate systems. The lateral and vertical distribution of calibrated seismic facies within this framework highlights the evolution through time of the carbonate system and bathymetry of the host lacustrine basin. Despite the simple, largely abiotic and microbial components, lacustrine carbonate accumulations formed complex geometries that closely resemble those observed from marine systems, suggesting that a downward-tapering carbonate production profile must have occurred. The complexity of the stratigraphic architecture reflects lateral variations in subsidence patterns combined with the interference of the basement topography, palaeo-wind directions and basinal filling patterns. Well-imaged clinoforms several hundred metres high attest to both the existence of significant lake-bottom topography, locally in excess of 800 m, and the occurrence of deep water at time of deposition. Platform margin trajectory and vertical and lateral architecture of clinoform packages through time reveal distinct sequence boundaries that can be correlated in detail only locally, demonstrating the impact of syndepositional tectonics, and possibly recurrent isolation of smaller lakes during lowstands. Depositional models from this study fill a gap in current understanding of lacustrine carbonate systems and offer a template for exploration and appraisal of the presalt play.

The Lower Cretaceous presalt carbonate units of the South Atlantic conjugate margins (Fig. 1, inset map) have proven to be a highly productive hydrocarbon play since the Tupy-1 (Lula field) discovery well in 2006. The presalt play consists of a prolific, lacustrine source rock, a widespread and thick carbonate reservoir and a thick capping salt interval that acts both as a world-class seal and as a heat buffer, preventing overmaturation of hydrocarbons. Although several large discoveries have followed Lula, a significant number of wells penetrated non-reservoir units, indicating that significant lateral heterogeneity in reservoir quality is one of the primary risks of the play, both in exploration and in development. For this reason, the presalt carbonate intervals have received considerable attention in the last decade from both industry and academia worldwide.

While the nature of the carbonate factory, whether microbial or abiotic (Carminatti *et al.* 2009; Wright and Barnett 2015; Kattah 2017; Liechoski de Paula Faria *et al.* 2017; Bastianini *et al.* 2019), and the bathymetry at time of deposition, whether flat and shallow or highly variable with deep water (Tremblay *et al.* 2014; Minzoni *et al.* 2017; Wright and Barnett 2017; Arienti *et al.*

2018; Wright and Rodriguez 2018; Simo *et al.* 2019), remains controversial, there is a general agreement that deposition occurred in dominantly lacustrine basins. These basins were laterally extensive and had very restricted, if any, communication with the open ocean. Because lacustrine carbonate systems have historically received far less attention than their marine counterparts, a plethora of studies have recently focused on the petrography of non-marine carbonate particles from both modern and ancient lacustrine analogues (e.g. Wright 2012; Della Porta 2015; Wright and Barnett 2015; Mercedes-Martín *et al.* 2017, 2019; and references therein). While these studies significantly advanced our knowledge of lacustrine carbonate systems, they also highlighted the uniqueness of the presalt section, in that thick accumulations of non-marine carbonate strata have no obvious modern or ancient analogues. Only a few recent studies have tackled the complex stratigraphy and seismic-scale architecture of the presalt carbonate interval (Buckley *et al.* 2015; Ceraldi and Green 2017; Saller *et al.* 2016; Minzoni *et al.* 2017; Arienti *et al.* 2018; Simo *et al.* 2019), and the understanding of the depositional, stratigraphic and tectonic elements that gave rise

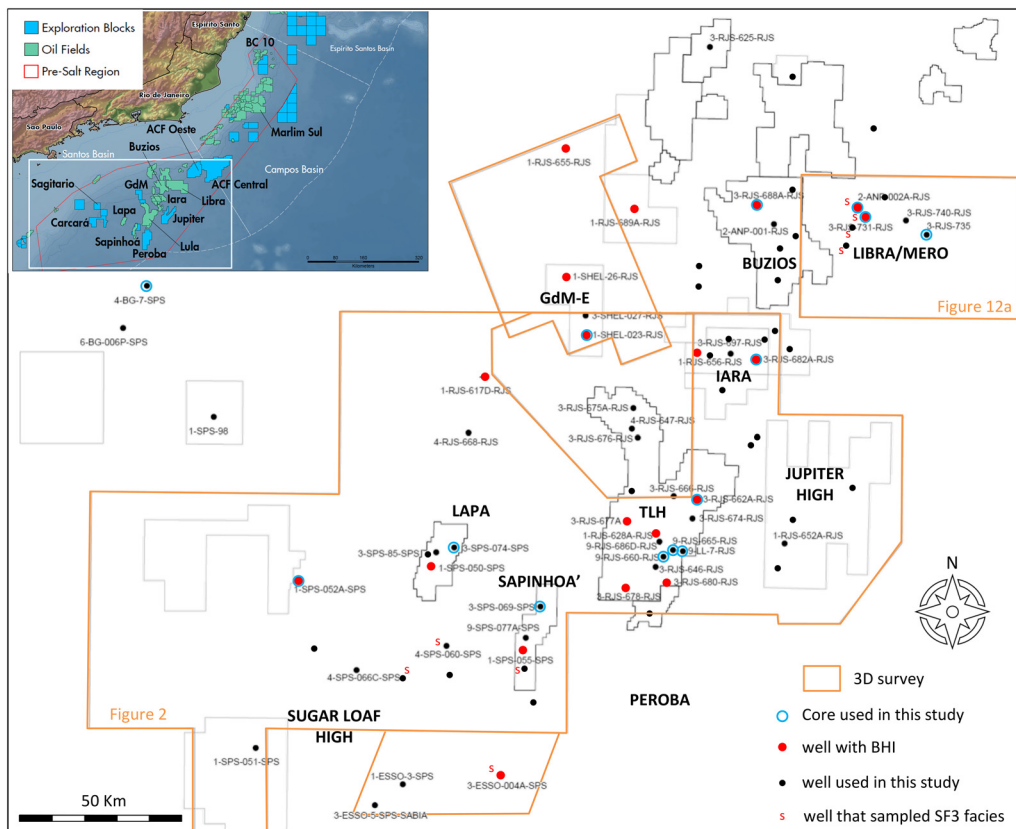


Fig. 1. Dataset used for this study, including 3D seismic surveys, wells, borehole images (BHI), and cores. Inset map: location of major presalt fields and exploration blocks within the Santos and Campos basins. White polygon indicates area of detailed study. TLH, Tupi–Lula High; GdM-E, Gato do Mato–Epitonium High; BHI, borehole images; ACF, Alto de Cabo Frio.

to the system has been notably sparse owing to confidentiality issues and a lack of detailed integration and calibration of data across scales. Recent efforts within Shell have focused on empirically characterizing the presalt carbonate interval in the Santos basin via an integration and calibration of mappable seismic facies with core, logs and borehole image data (BHI; Figs 1 & 2).

Here we summarize the extensive observations conducted at the Shell Exploration and Technology Laboratory, between 2007 and 2016, to highlight the sequence stratigraphic architecture of presalt carbonate systems of Brazil and discuss both local and basin-wide controls on their stratigraphic evolution, as well as the palaeobathymetry of the presalt lake system. For confidentiality reasons, this paper does not disclose any detail on well or core data, except for their location. As a prime example of the basin evolution in offshore Brazil, this study focuses principally on the sag interval (the primary reservoir) of

the Santos Basin, where good-quality CGG Pre-Stack Depth Migrated (PSDM) volumes were available (Figs 1 & 2).

Geological setting and regional stratigraphy

Carbonate deposition in the presalt section of Brazil started in the Early Cretaceous period, during the late phase of the south to north, multiphase rifting event (which spanned from Late Jurassic to Early Cretaceous) that separated South America from Africa. It continued through the transition and post-rift, thermal subsidence (sag phase), associated with continent breakup and onset of a passive margin (Fairhead and Wilson 2005; Davison 2007). Rifting in the Santos Basin occurred in several phases, which are separated by regional unconformities (Fig. 3). Early rift stratigraphy consists of a thick interval of volcanic and siliciclastic units (Camboriú and

Seismic architecture of lacustrine presalt carbonate systems

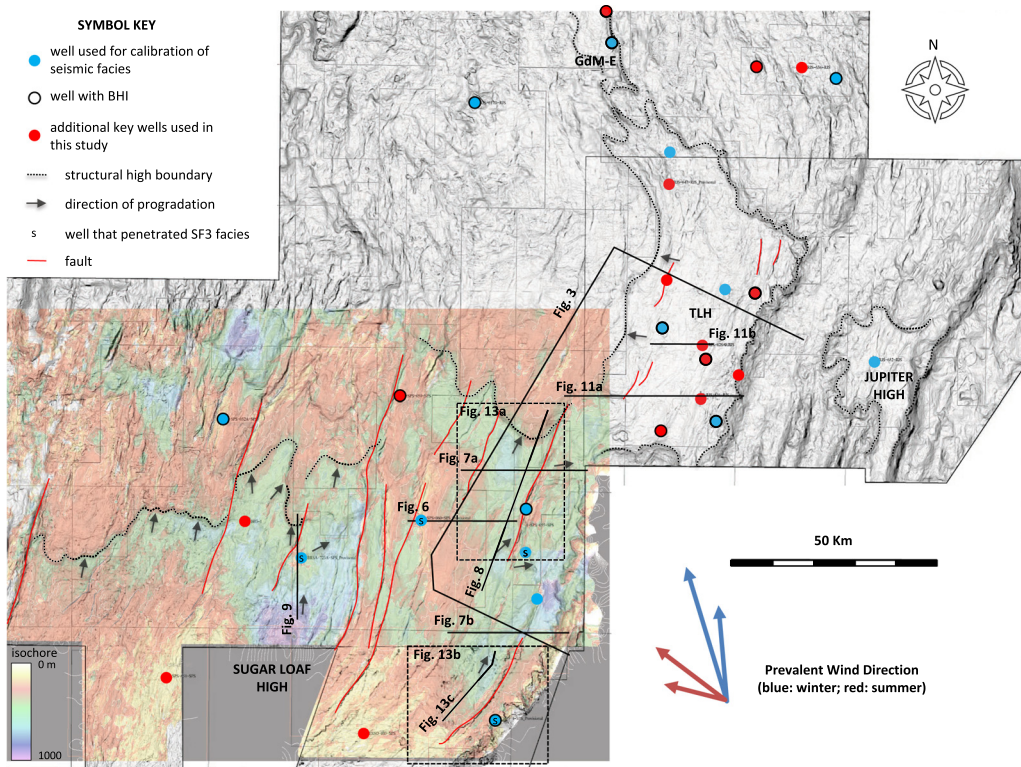


Fig. 2. Semblance map of the base salt showing the details of the morphology of the carbonate shelves over the Sugar Loaf High and the Tupi–Lula High (TLH). Structural high boundaries are marked with a dotted line. The Sag (Upper Barra Velha) isochore map is also shown over the Sugar Loaf High. Note that thick sediment packages (green, blue, and mauve) correspond to prograding wedges (see Figs 6–9 & 13), while shelf tops and basins are areas of thin to null sediment accumulation (red and yellow), indicating sediment starvation or erosion in those areas. Arrows indicate direction of progradation. Note also null sediment thickness along the SE margin in correspondence to arcuate features interpreted as collapse margin and bypass slopes. GdM-E, Gato do Mato–Epitonium High; BHI, borehole images

Picarra formations; Fig. 3) associated with the Paraná rift volcanism and initial erosion of basement rocks composed of metasediments.

Carbonate shelves, platforms and ramps of the Itapema and Barra Velha formations (Minzoni *et al.* 2017; Simo *et al.* 2019; Fig. 3) developed initially on local, basement-cored highs, with intervening lows accumulating volcanic and deeper water deposits, which are inferred to contain at least part of the regional source rock intervals. A general inference from well data is that most coeval, coarse clastic settings were confined to inboard, proximal areas, with cleaner carbonates developing atop outboard basement blocks (Davison 2007; Muniz and Bosence 2015).

The regional presalt stratigraphy has been extensively reviewed in several studies (e.g. Pereira and Feijó 1994; Dias 2005). The presalt across the entire South Atlantic is subdivided into a number

of mega-sequences. The latest stratigraphic chart for the Santos Basin was issued by Moreira *et al.* (2007) after the drilling of the first presalt wells in the São Paulo Plateau in deep waters of the Santos Basin.

The presalt carbonate section in the Santos Basin consists of two main carbonate factory types. Coarse molluscan rudstone, grainstone and packstone of the Itapema Formation, commonly known as ‘coquina’, is widely described from the upper rift section, especially in the Campos Basin, offshore Brazil, and the conjugate West African basins (e.g. Guardado *et al.* 1990; Mello *et al.* 2002; Carminatti *et al.* 2008). The overlying Barra Velha Formation is a mix of carbonate mudstones, spherulitic calcite wackestones and packstones (locally dolomitized), shrub-dominated framestones and grainstones composed of reworked elements of the various carbonate and volcanic lithotypes in the basin (e.g. Rezende and Pope 2015; Wright and Barnett 2015, 2017; Minzoni *et al.*

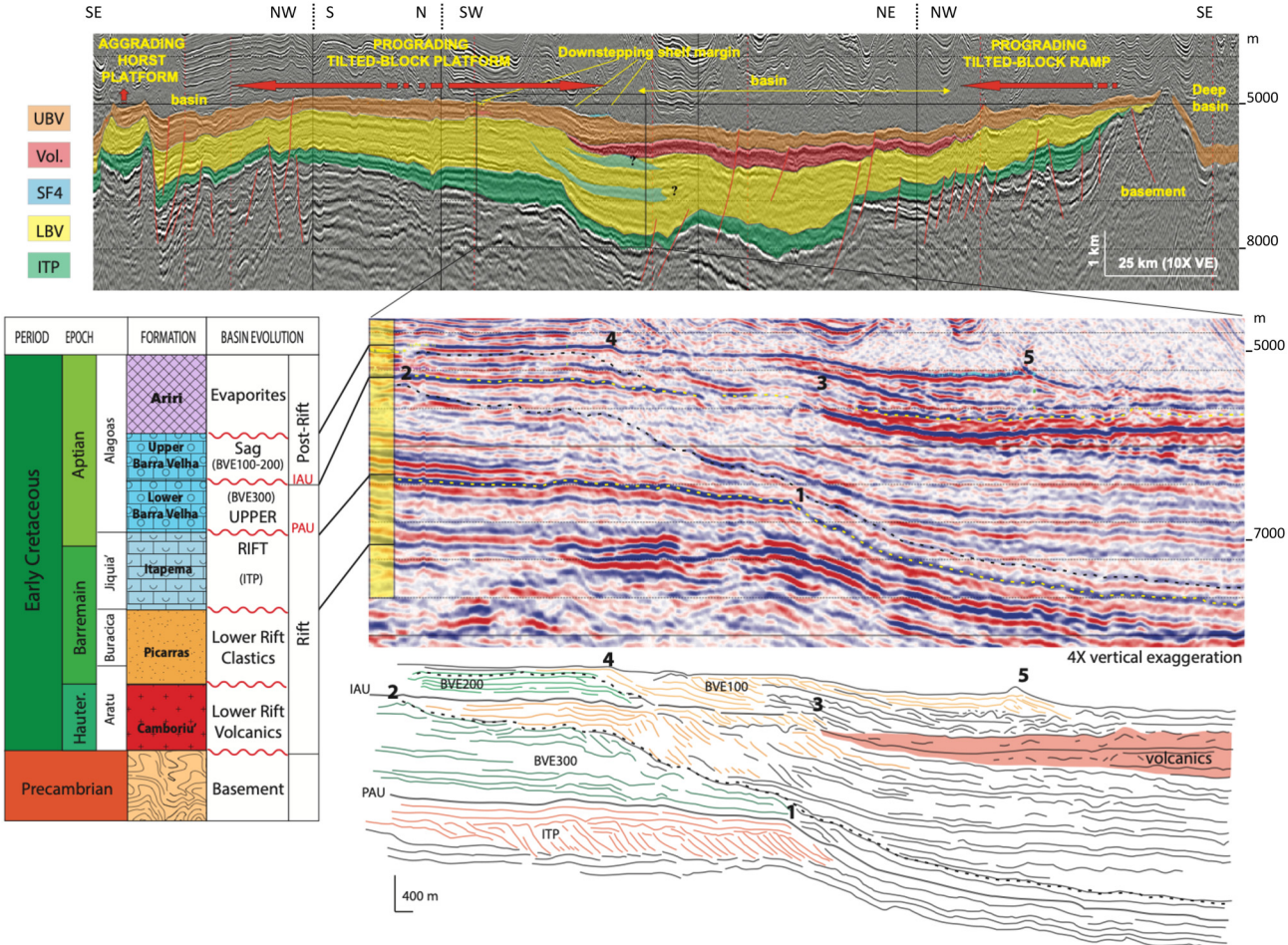
M. Minzoni *et al.*

Fig. 3. Line drawing and interpreted regional and representative seismic section for the Santos Basin, and stratigraphic chart of the Itapema and Barra Velha systems. Green and orange lines in the detailed section represent aggradational-backstepping and progradational-downstepping units, respectively. The yellow hatched lines mark the regional unconformities (IAU and PAU); black hatched lines mark the boundary between major aggrading and prograding units. See Figure 2 for location. Wavy red lines in the stratigraphic chart indicate regional unconformities. IAU, Intra-Alagoas Unconformity; PAU, Pre-Alagoas Unconformity; UBV, Upper Barra Velha; LBV, Lower Barra Velha; ITP, Itapema; Vol., volcanics. Numbers 1–5 in both the seismic line and the line drawing indicate the position of the margin through time.

Seismic architecture of lacustrine presalt carbonate systems

2017; Arienti *et al.* 2018; Souza *et al.* 2018). The abiotic carbonate component of the Barra Velha is composed almost entirely of calcite crystal shrubs and spherulites, either in place or reworked, and locally thick and laterally continuous accumulations of carbonate mud (Wright 2010; Wright and Barnett 2015); Mg-silicate clay is variably present in all lithotypes, but is most typically associated with spherulitic wackestones and packstones.

Although the exact origin or carbonate factory of the sag interval, whether truly microbial, microbially induced, or abiotic, is a matter of debate, the upper rift and the sag are characterized by distinct factories that differ not only in terms of components, but also in their mode of carbonate accumulation that presumably reflects a drastic change in water chemistry owing to a progressive increase in restriction, salinity and alkalinity (Pietzsch *et al.* 2018). Conceptual models and analogue studies from marine systems indicate that different carbonate factory types are associated not only with different porosities and permeability distributions, but also with different large-scale stratigraphic architectures (Pomar 2001; Schlager 2005; Della Porta *et al.* 2013; Minzoni *et al.* 2013). The same concept and relationships are likely to be applicable to lacustrine systems, where variations in water chemistry are more extreme and should result in even larger variations in carbonate factory types and stratigraphic architectures.

Data and methods

Seismic stratigraphy and seismic facies were interpreted and mapped on both regional 2D lines over the Campos and Santos basins and on a large CGG PSDM 3D volume covering the entire 'Cluster Area' (Sugar Loaf High, Tupi–Lula High, Iara and Jupiter High), along with the addition of smaller volumes over the Libra, Peroba and Buzios – Gato de Mato–Epitonium – areas (Figs 1 & 2). Mapping over the larger cluster area was aided by the analyses of amplitude, semblance and isochore maps extracted from key seismic stratigraphic surfaces. Mapping over Libra also included observations on root mean square amplitude maps and application of a Van Gogh filter to minimize directional noise.

Observations on seismic facies and seismic unconformities were calibrated with >100 wells, regionally distributed over the Campos and Santos basins and containing standard petrophysical data, core and rotary sidewall core samples, as well as borehole images. This study focuses on the Santos Basin and builds on the analysis and integration of 2D and 3D seismic data with 79 wells, including 19 with BHI logs, and 14 cores with a cumulative core thickness of approximately 1000 m. A total of 16 wells were tied to the seismic trace and used for

detailed calibration of the seismic facies (Figs 1 & 2; Table 1). All of the seismic facies types (Table 1) described in this study were tied to wells using both BHI and core material from at least one location, commonly more. At this time the BHI logs cannot be reproduced owing to confidentiality limitations.

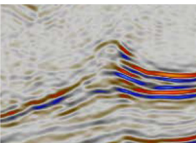
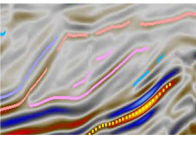
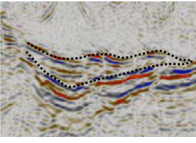
The major unconformities were identified in seismic volumes, calibrated with well data and correlated regionally. The base salt is a high-amplitude peak reflector that can be correlated across basins. The Intra-Alagoas Unconformity (IAU or base sag; Fig. 3) is prominent on palaeohighs but can appear conformable in palaeodepressions. The Pre-Alagoas Unconformity (PAU; Fig. 3) is interpreted as the switch from rifting to a transitional phase. It is a seismic angular unconformity only locally, where significant tilting of underlying strata occurred.

The calibration of seismic facies consisted of an initial analysis and identification of reflector packages near the wellbores for each tied well. Each individual seismic facies zone in the well was identified by a top and a bottom based on the geometric attributes of the reflection packages (see Table 1) and confirmed with BHI data where available. These intervals were then compared with both well- and core-based facies associations to help calibrate the lower resolution seismic interpretations with the higher-resolution, well-based observations. Comparisons between these two different methods generally showed good agreement, validating the seismic facies as good proxies for depositional facies and thus environment of deposition. For example, SF3 facies identified in seismic images and consisting of inclined reflectors were confirmed by inclined stratal packages observed in BHI. Where discrepancy occurred, further iterations of near-wellbore seismic facies identification were performed with corrections made where interpretational ambiguity existed.

Owing to major differences between the carbonate factories characterizing the Itapema and Barra Velha depositional systems, dominated by coquina and microbial–abiotic carbonate rocks, respectively, and the sparse calibration data for the rift system, only a basic workflow was applied to the Itapema Formation. This workflow relied primarily upon well data and seismic-derived maps, rather than detailed line-by-line, gridded seismic facies interpretation as was done for the Barra Velha interval.

Detailed mapping of seismic facies was performed on the sag interval (Upper Barra Velha) only. Seismic reflection packages are classified into four main seismic facies according to their external geometric attributes and are interpreted based on the attributes of the internal reflectors and their position within the depositional profile (Table 1). Scrupulous attention was applied to the interpretation of SF1 and SF3 facies (mounded and inclined, respectively; Table 1) by carefully testing for residual

Table 1. Seismic facies (SF) classification scheme, description, occurrence and interpretation of seismic facies

Seismic facies	External geometry	Example	Variation	Occurrence				Lithofacies	Interpreted depositional environment
				Top	Margin	Slope*	Lows*		
SF1	Mounded (convex upward)		Shingled	× ×	× × ×			Grainstone	Marginal shoals; islands
			Chaotic	× ×	× × ×	× ×	×	Shrubs; boundstone; grainstone	shallow and deep water 'reefs' / buildups; islands; deep water MTDs
			Transparent	×	× × ×	×	×	Volcanics; grainstone; boundstone	Volcanics; shallow and deep water 'reefs' / buildups; islands
SF2	Tabular		Parallel	× × ×	× ×			Packstone; wackestone; grainstone	Shelf top deposits; 'lagoon'; basinal or profundal deposits
			Chaotic*	×				Volcanics	Shelf-top breccia; volcanics
			Parallel						
SF3	Inclined		Progradational		× × ×	× ×		Not tested	Bypass slope
			Chaotic			× ×		Packstone; wackestone	Accretional slope
SF4	Wedged		Chaotic			× ×		Rudstone [†]	Accretional slope
			Converging*			× × ×		Laminates	Lower slope MTDs
								packstone	Lower slope MTDs and turbidites

^{*}Poorly tested.[†]Itapema ('coquina') unit only.
MTDs, Mass transport deposits.

Seismic architecture of lacustrine presalt carbonate systems

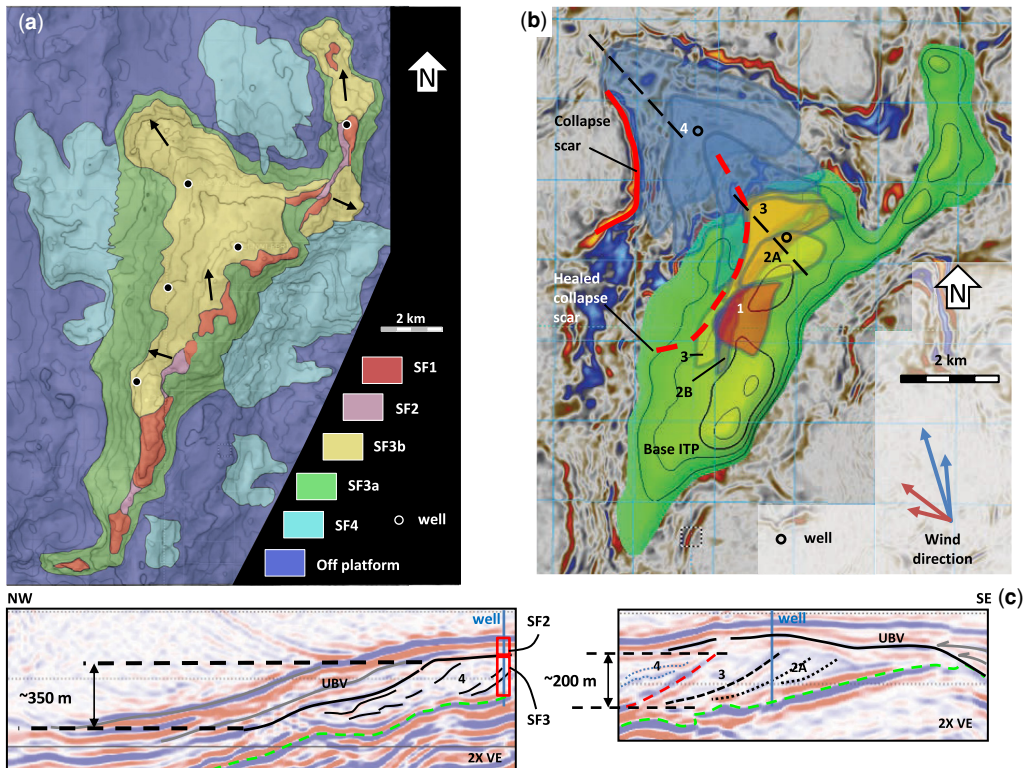


Fig. 4. Upper Rift seismic facies and slope geometries over NW Libra (Mero). (a) Seismic facies map below the Intra-Alagoas Unconformity (contour lines). Note dominance of SF3 facies, and dimensions, orientation and distribution of SF1 (mounded) facies. (b) Details of fan-shaped SF3 facies and their evolution through time (1–4) from top of structure down to the NW flank. Note the prominent sector-collapse feature cutting through fan 3 and healed by fan 4. Note also a second collapse scar cutting through fan 4. (c) Interpreted seismic sections, oriented NW–SE, through the fan system (hatched lines in Fig. 4b). The fans are stacked laterally and downstep from the top of the structure to the NW flank. Note the steep angle of the prograding clinoforms penetrated by the wells and the increasing height of the clinoforms as the system progrades down a tilted basement into deeper water. Accumulation of prograding clinoforms limited to the northwestern end of the structure may indicate drifting of slope sediment northward by deep currents. Note also the progressive onlap of the Upper Barra Velha onto the underlying Upper Rift. The green hatched line marks the base of the Itapema. UBV, Upper Barra Velha; ITP, Itapema.

pullup artefacts and multiples from the overlying salt by comparing the reflection geometries in both intervals in map and cross-section view. Mapping of inclined facies (SF3) was locally facilitated by flattening at toplap or downlap surfaces over very limited areas, and by applying a stratal convergence attribute (Lomask *et al.* 2009; van Hoek *et al.* 2010).

Seismic stratigraphic architecture and morphology

The geometry and termination patterns of seismic reflections can be used to extract a general sequence stratigraphic frame (e.g. Mitchum *et al.* 1977) and

also to interpret the morphological evolution of carbonate accumulations (e.g. Bachtel *et al.* 2004). The lateral and vertical distribution of seismic facies within this framework highlights the stratigraphic evolution of the presalt carbonate systems in the Santos Basin.

The position of lacustrine coastal onlap within the defined seismic stratigraphic framework can be used as a proxy for foreshore environments and thus its position through time records base-level fluctuations (Vail 1987; Buckley *et al.* 2015). The shelf or platform margin marks the boundary between two very distinct settings, with the subhorizontal area (or platform top) being dominated by autochthonous deposition and relatively minor reworking from storms

and currents, and the slope being dominated by gravity and deep current processes. These general characteristics, which have been widely documented in marine systems, are also observed in cores that penetrated the lacustrine presalt section, although the detailed interpretation of depositional settings is complicated by the unusual nature of the specific facies. In general, platform or shelf margin facies are dominantly grain supported or are composed of autochthonous precipitates, whereas slope facies and protected, slightly deeper, shelf areas away from the margin contain a markedly higher abundance of mud- and Mg-clay-dominated textures (Table 1; Fig. 4c; see also Figs 1, 2, & 4a for location of wells that penetrated SF3 facies interpreted as slope). The position of the shelf margin, whether truly marking base level or not, can therefore also be used as a proxy for base-level fluctuation, with the advantage of being easier to identify than coastal onlaps in seismic images. Platform and shelf margins in the presalt Santos are geometrically identified in seismic images by the slope break that separates originally subhorizontal and parallel reflectors (SF2 facies) from inclined or wedged reflectors (SF3 and SF4 facies; Table 1), and can be classified as retrogradational/backstepping, aggradational, progradational, and downstepping (Fig. 3).

Despite the complexity of the stratigraphic architecture of the presalt section in the Santos Basin, a few general sequence-stratigraphic observations can be extracted for the relatively better studied and more widely distributed upper synrift and sag Itapema and Barra Velha intervals.

Itapema

The Itapema interval is here defined tectono-stratigraphically as the lower part of the synrift interval bounded at the base by a reginal transgression that marks the inception of carbonate deposition, and at the top by the PAU (Fig. 3; Moreira *et al.* 2007; Winter *et al.* 2007; Buckley *et al.* 2015; Pietzsch *et al.* 2018). The Itapema Formation is informally known as the ‘coquina’ and has equivalences in the Campos Basin to the north (Fig. 3). Across the study area the stratigraphy of the Itapema interval is based primarily on interpretation of seismic reflection data; well and core calibration was mainly limited to the Libra structure (Figs 1 & 2). With the exception of Libra, carbonate systems are largely untested in this interval, but seismic data indicate general progradation of inclined reflectors (SF3; Table 1) during this time for the greater Santos area (Fig. 3). Although poorly constrained, details of the stratigraphy of the Itapema are important to understanding carbonate reservoir distribution in Libra and other prospects in the northern part of the Santos Basin, as well as the Campos

Basin to the north and the equivalent section in the conjugate West African margin, where the upper rift ‘coquina’ is the major producing reservoir (Guaraldo *et al.* 1990; Mello *et al.* 2002; Carminatti *et al.* 2008; Saller *et al.* 2016; Barnett *et al.* 2020).

The Itapema in the North Santos occurs over relatively small but high-relief basement blocks, a few kilometres across and up to 800 metres high, and consists of a thick interval of inclined facies (SF3; Table 1), connecting very thin or null platform tabular-parallel facies (SF2; Table 1) at the top of the basement blocks to off-platform tabular-parallel facies (SF2; Table 1) with variable thickness (Fig. 4). This package records strong progradation with toplap and downlap geometries, which are indicative of minimal to negative accommodation at the platform top (Fig. 4). Local downstepping (Figs 3 & 4) indicates forced-regression and progressive base-level fall during later depositional stages of the interval. Detailed mapping reveals that the bulk of the deposition over the NW sector of Libra occurred as a relatively localized series of leeward progradational fan- and lobe-shaped geobodies, possibly reworked by longshore currents during lowstands (Barnett *et al.* 2020) or by deeper-water currents during highstands (Fig. 4).

Mounded facies (SF1; Table 1) within the upper rift interval are relatively extensive, up to 3 km long and several hundred metres wide, and up to several tens of metres thick (Fig. 4a). The upward-convex reflector packages are commonly internally chaotic or transparent, and rooted onto the underlying topographic highs, usually lining rift shoulders and windward margins. Less common SF1 facies occurring atop progradational facies are generally characterized by internal shingled reflections.

Volumetrically, the Itapema at Libra is almost exclusively composed of inclined facies (SF3; Table 1) with limited mounded facies (SF1; Table 1) and very limited tabular-parallel facies (SF2; Table 1; Fig. 4a). Inclined reflector packages are progradational, internally chaotic and steep (up to 18°; Fig. 4c), suggesting that the clinoforms are composed of coarse shell fragments (coquina), but with local sedimentation breaks represented by hardgrounds or clay-rich intervals as highlighted by high internal reflectivity and confirmed by lithological observations from core samples (Barnett *et al.* 2020). The stratigraphic top of the Itapema is characterized by large arcuate scar features that extend up to 4 km along the shelf break and 1 km shelfward (Fig. 4), and by linear channel-shape structures, about 2 km long, at the base of slope that run perpendicular to the shelf margin (Fig. 5). These features are interpreted, respectively, as margin collapse and weak channelization at the base of slope, a feature commonly observed in grain-dominated carbonate slopes (e.g. Playton *et al.* 2010). Basinward

Seismic architecture of lacustrine presalt carbonate systems

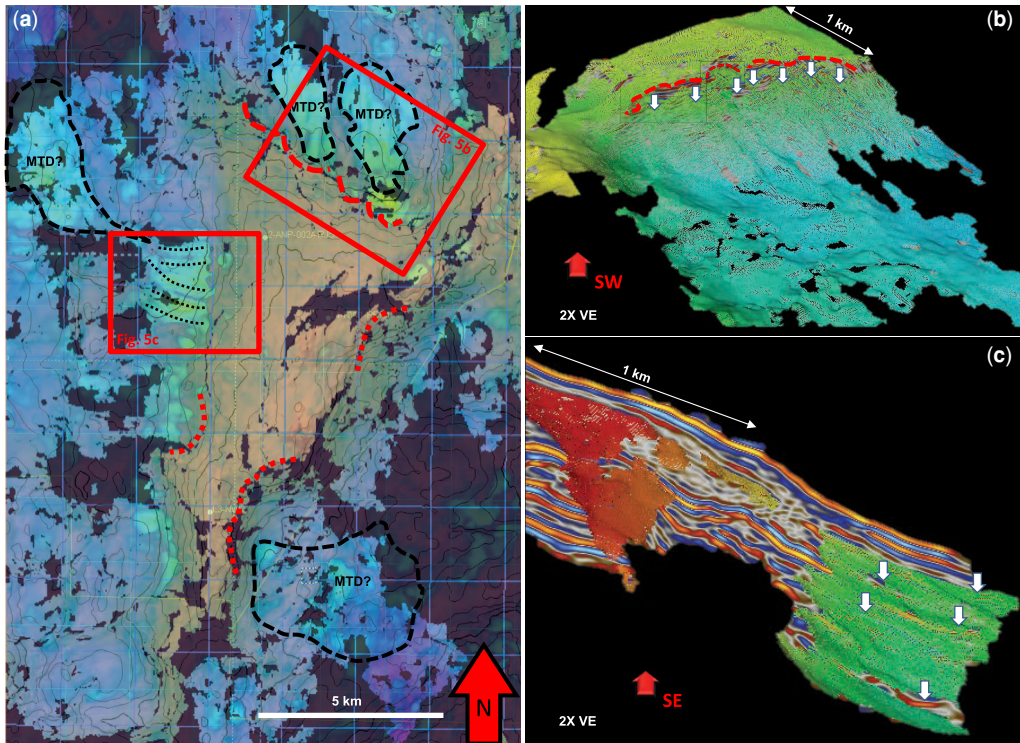


Fig. 5. Morphology of Upper Barra Velha BVE100 clinoforms around Libra (Mero field) as recorded by picked Sag horizon surfaces along inclined reflectors flanking the Libra structure. (a) Combined top sag (base of salt) structure map and root mean square (RMS) attribute over NW Libra. Note arcuate reentrances along the margin (dashed red lines), interpreted as sector collapse scars, and associated bright RMS features along the slope and proximal basin interpreted as channels and mass transport deposits. (b) Horizon extraction at base salt showing slope clinoform along the steeply dipping side of a tilted block. Note collapse scars (red dashed line) and channelized upper slope (white arrows). Note also the exponential shape of the clinoform. Dip angle is about 25°. (c) Horizon extraction at the top of Itapema showing slope clinoform along the hanging wall, gently dipping side of a tilted block. Note channel features (white arrows) in the lower slope and overall sigmoidal shape. The lower slope channel features are also seen in Figure 5a at the base of the salt as elongated, bright features perpendicular to the margin in the RMS attribute (dotted lines). Dip angle is c. 10°.

progradation (away from the underlying palaeohighs) only partially filled the accommodation available at the slope, so that at the end of deposition, the platform maintained a high relief (up to several hundreds of metres) over the surrounding basin (Fig. 4c).

Lower Barra Velha (BVE300)

The BVE300 interval corresponds lithostratigraphically to the lower part of the Barra Velha Formation, below the IAU (Fig. 3; Moreira *et al.* 2007; Buckley *et al.* 2015; Pietzsch *et al.* 2018) and marks the first appearance of in-situ microbial/abiotic framework.

Localized mounded facies (SF1; Table 1) are mapped throughout the basin, mostly aligned with basement structures and on top of rift shoulders

(Figs 4a & 6). SF1 facies are commonly stacked vertically to form larger composite mounds up to a few hundred metres thick and up to 1 km wide (Fig. 6). Mounded facies developed along hanging walls are locally characterized by a distinct backstepping trend (Fig. 3). Along a large sector of the Sugar Loaf High, however, the stacking pattern of the SF1 facies and shelf margins within an expanded section of the BVE300 displays a full cycle that includes backstepping and aggradation in the lower part, followed by progradation of clinoform wedges (SF3; Table 1) in the upper part (Fig. 3).

Additional mounded and wedged chaotic reflectors (SF1 and SF4; Table 1) adjacent to the platform complexes are interpreted as re-deposited carbonate strata that contributed to the infill of the troughs during the latest stage of the synrift phase (Fig. 3).

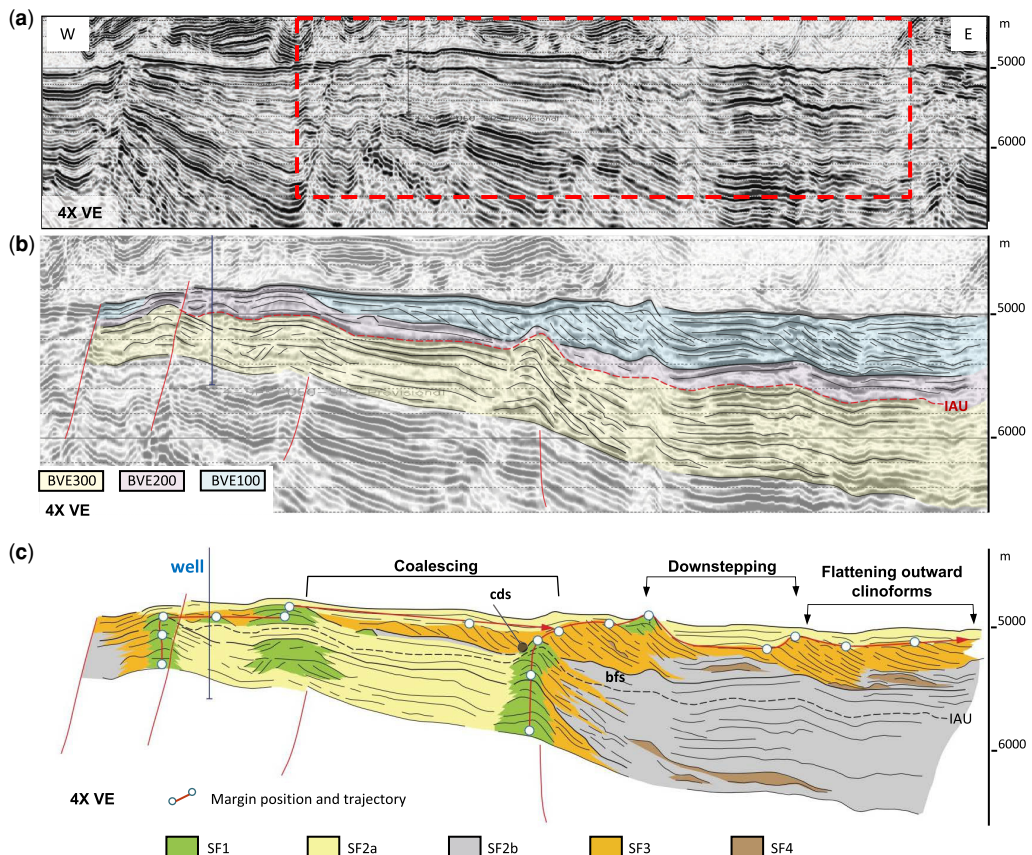


Fig. 6. East–west seismic line through the Sugar Loaf High showing the synrift to post-rift stratigraphic evolution of the presalt carbonate system. See Figure 2 for location. (a) Uninterpreted seismic line. (b) Interpreted detail of the line in (a) with interpreted stratigraphic architecture. (c) Interpretation of seismic facies architecture showing asymmetric aggradation on rotating fault blocks during the BVE300 and BVE200 intervals v. distinct progradation and downstepping during BVE100 deposition. Note the different slope geometry between the Lower Barra Velha BVE300 (interfingering with basin-filling reflectors) and in the Upper Barra Velha BVE100–200 (downlap over a starved basin). Note also the vertical stacking of SF1 facies in the BVE300 interval. The control well penetrates three different seismic facies. IAU, Intra-Alagoas Unconformity; bfs, basin infilling strata; cds, climbing downlap surface.

Basinal sediment infill during the BVE300 was localized and impacted slope geometries and platform progradational patterns by partially filling the basin and reducing accommodation at the toe of slope (Minzoni *et al.* 2017; Fig. 6). A large area within the palaeovalleys was filled by volcanic rocks and volcanoclastic sediment (Fig. 3), as suggested by gravity and magnetic data, highly reflective seismic loops, and confirmed by several wells that penetrated this interval. Evidence of pillow-lava structures, hydrovolcanic breccias and palagonitized volcanic glass recorded in borehole images (De Luca *et al.* 2015) indicate that at least part of the volcanic strata in the Santos Basin were deposited

subaqueously; however, the lateral continuity of parts of these extrusive bodies as mapped from seismic suggests that much of the interval accumulated as subaerial flows.

Upper Barra Velha (BVE100 and BVE200)

BVE200 and BVE100 are here defined sequence-stratigraphically, based on seismic unconformities, reflector geometries and terminations, and seismic facies distribution. The base of the BVE200 is a high-amplitude peak reflector marking the IAU and corresponds to a transgressive surface over the BVE300 as indicated by local progressive onlap of

Seismic architecture of lacustrine presalt carbonate systems

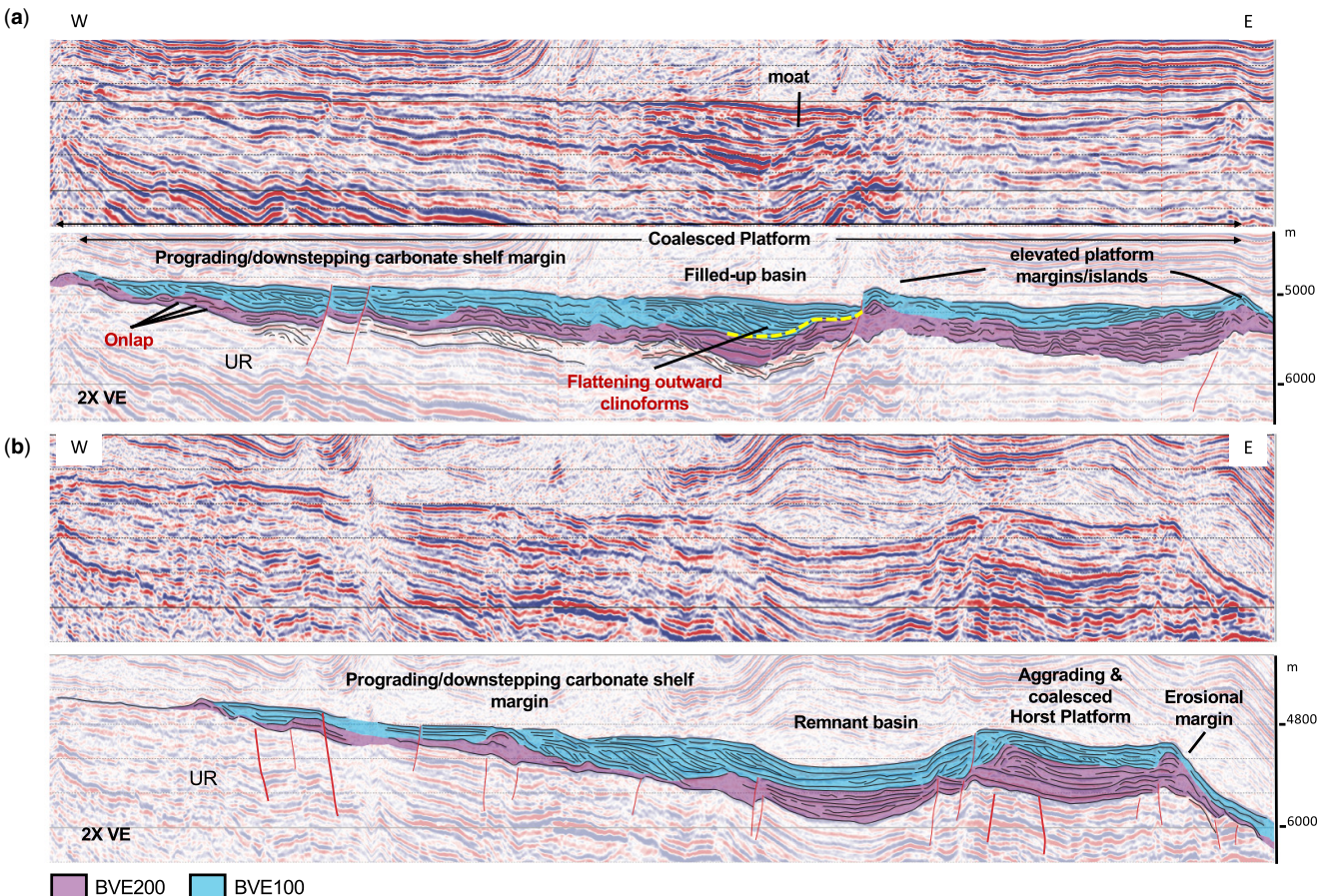


Fig. 7. Uninterpreted and interpreted seismic sections over the Sugar Loaf High (Santos Basin). See Figure 2 for location and Figure 3 for stratigraphy. (a) Progradation of the BVE100 shelf margin in the interior of the large structural high vast areas of local basins by coalescing with horst-top aggrading BVE200 and BVE100 platforms, or (b) terminated before reaching the horst structure leaving an unfilled remnant basin. Note progressive onlap of the BVE200 onto the Upper Rift. UR, Upper Rift (Itapema and BVE300).

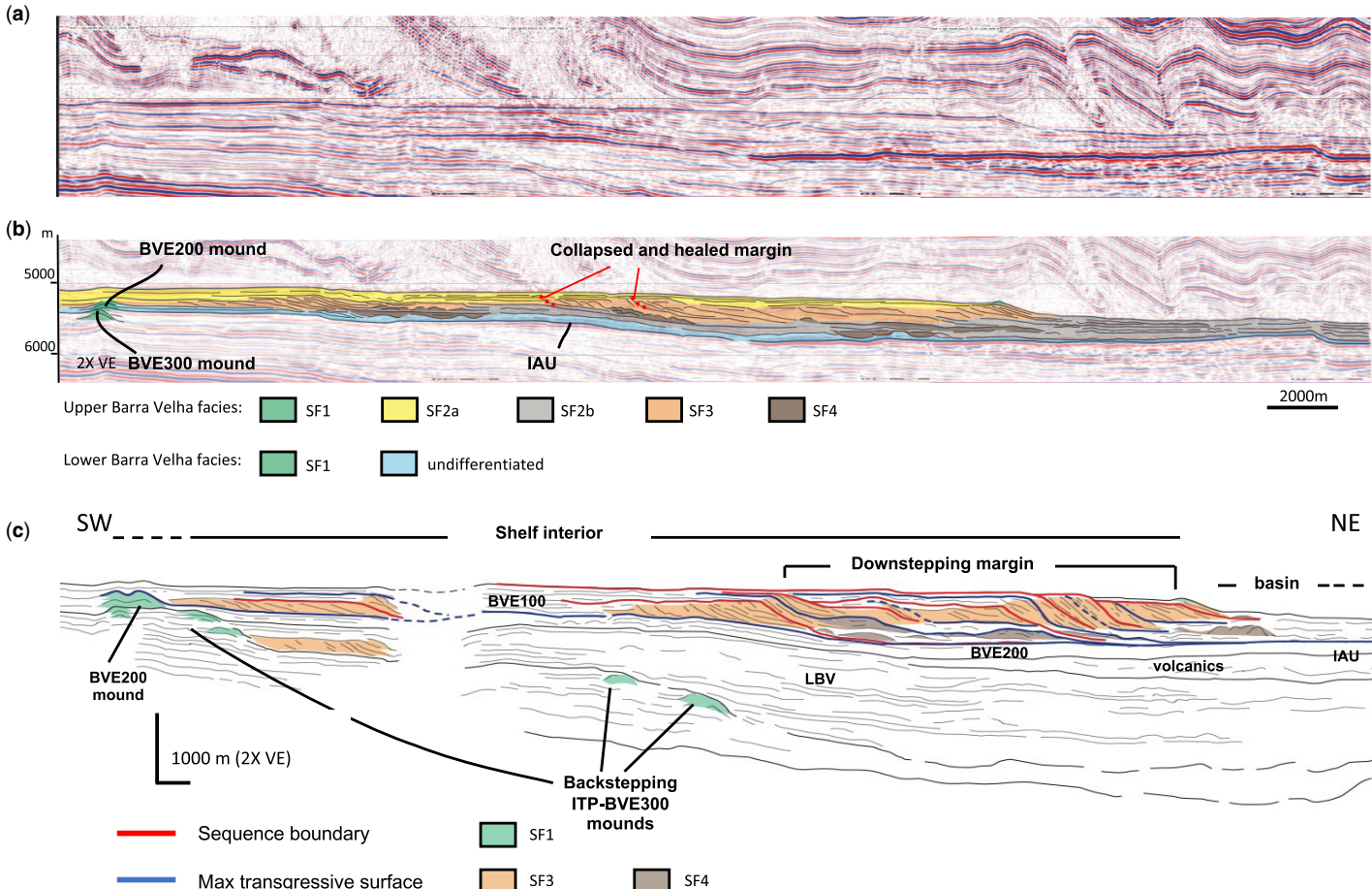
M. Minzoni *et al.*

Fig. 8. Slope geometry, margin trajectory, facies distribution, and sequence stratigraphic architecture of the BVE units over the Sugar Loaf High. Uninterpreted (a) and interpreted (b) seismic line of the Upper Barra Velha interval. (c) Higher-order sequence stratigraphic boundaries interpreted from reflector terminations and seismic facies within the BVE100 interval. See Figure 2 for location and Figure 3 for stratigraphy. IAU, Intra-Alagoas Unconformity.

Seismic architecture of lacustrine presalt carbonate systems

seismic reflections on the underlying upper rift interval (Buckley *et al.* 2015, their figure 3; Figs 4 & 7). Accordingly, areas of prevalent aggradation in the Upper Barra Velha are limited to the BVE200 (Figs 3 & 6–9). Aggrading margins at block shoulders produced vertically stacked mounded facies (SF1; Table 1) with significant depositional relief (up to about 200 m) that is commonly onlapped and filled by distal slope facies of BVE100 prograding units (Upper Sag; Figs 6 & 7). This geometry, known as climbing downlap surface, implies that the initially aggrading system was unable to prograde when subsidence rates dropped, probably owing to a pre-existing, unfilled topographic relief or a windward position, and that sediment created during deposition of the BVE100 was transported laterally to downlap the mounds (Minzoni *et al.* 2017; Fig. 7a).

The base of the BVE100 is placed at the aforementioned downlap reflector surface and correlative surfaces. It therefore coincides with a composite maximum flooding or regressive surface in the classic sequence stratigraphic models (Galloway 1989; Schlager 1989, 2005; Mitchum and Van Wagoner 1991; Catuneanu *et al.* 2009). The BVE100 is dominated by prograding to downstepping stacking patterns, which imply little to negative

accommodation on palaeohighs (Tremblay *et al.* 2014; Minzoni *et al.* 2017; Figs 6–9). In detail, however, the strongly progradational pattern is punctuated by episodes of aggradation that define distinct sequences (Buckley *et al.* 2015; Minzoni *et al.* 2017; Fig. 8).

Prograding clinoforms are generally steep (8–12° average) and linear to exponential, suggesting a possible dominance of coarse-grained sediment or *in-situ* boundstone accumulation on the upper slope (Adams and Kenter 2013; Minzoni *et al.* 2017; Figs 9–12). Where progradation occurs over a shallowing upward basin or downlaps onto a relative palaeohigh, such as in coalescing margins (Eberli and Ginsburg 1987), the clinoforms display a flattening outward geometry (Bosellini 1984) and a shift from planar to tangential profiles (Figs 6, 7a, 9 & 10a). In plan view, the clinoform packages show very intricate geometries with internal erosional and reactivation surfaces. In areas of complex topography with promontories and embayments, the clinoforms display a distinctly arcuate accretion geometry (Fig. 13), similar to that observed in modern marine and lacustrine strand plains, where beach ridges accrete through storms and drift currents (e.g. Thompson and Baedke 1997; Goodfriend and Stanley 1999; Tremblay *et al.* 2014; Minzoni *et al.* 2017).

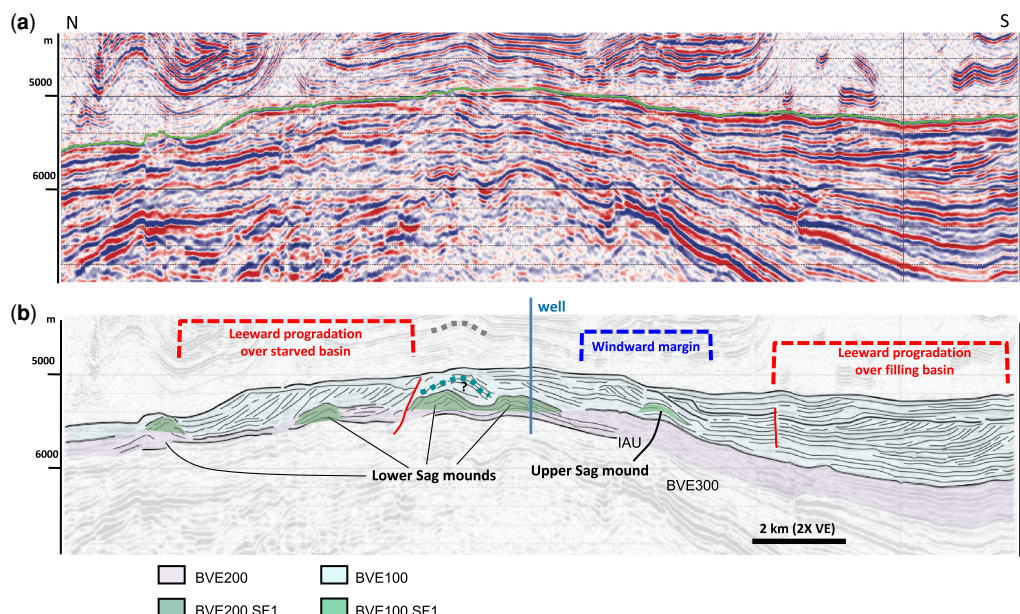


Fig. 9. Uninterpreted (a) and interpreted (b) seismic lines of the Upper Barra Velha interval over the southern part of the Sugar Loaf High. See Figure 2 for location and Figure 3 for stratigraphy. The asymmetry of the margin is interpreted as windward–leeward effect. Note the flattening outward profile of the clinoform wedge to south. Note also that the control well penetrates parallel, inclined and mounded reflectors of the BVE100–200 interval. Continuation of BVE200 mounded (SF1) facies into the BVE100 near the well location is possible but note that the mound shape mimics reflections in the salt above. IAU, Intra-Alagoas Unconformity.

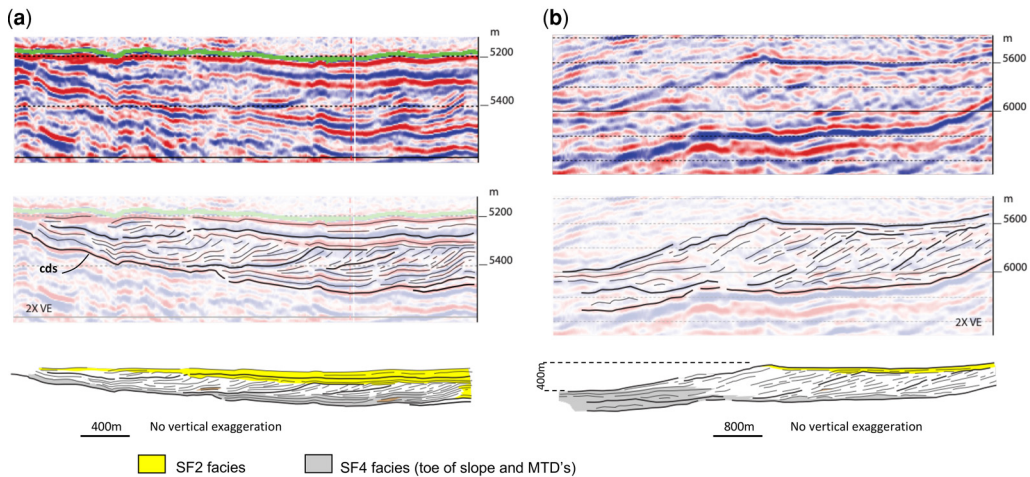


Fig. 10. Principal slope morphology types of the BVE100 prograding interval. (a) Climbing and exponential geometries of the prograding slopes over filling basin and onto a palaeohigh. Note also the flattening outward profile. (b) Tabular and linear geometry of the prograding clinoforms over unconfined, sediment starved basin. cds, climbing downlap surface.

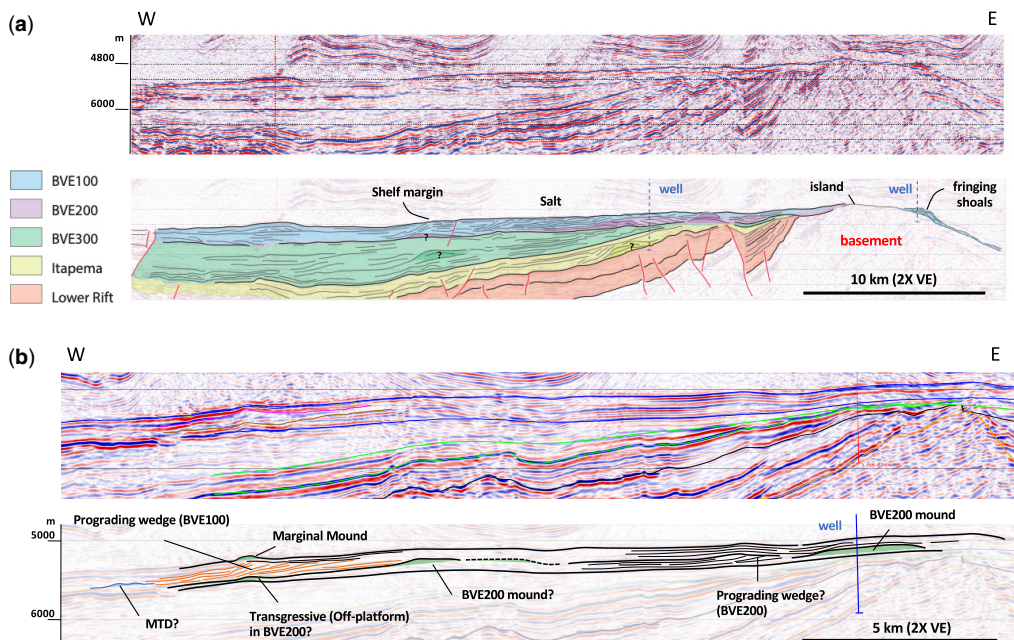


Fig. 11. Uninterpreted and interpreted seismic lines over the Tupi–Lula High. See Figure 2 for location. The black hatched line in (b) marks the potential extension of a BVE200 mound into an area disrupted by multiples from the overlying salt. Note backstepping of SF1 (mounded) facies during deposition of the BVE200 interval and progradation of inclined reflectors (SF3) during deposition of the BVE100 interval. Note also asymmetric progradation on the leeward (west) and shallow basin compared with lack of significant progradation along the steep and deep windward margin (east) in (a). The control well to the west of the island in (a) records significantly higher proportion of shale and fine sediment in the BVE100 than the well to the east. MTD, mass transport deposit.

Seismic architecture of lacustrine presalt carbonate systems

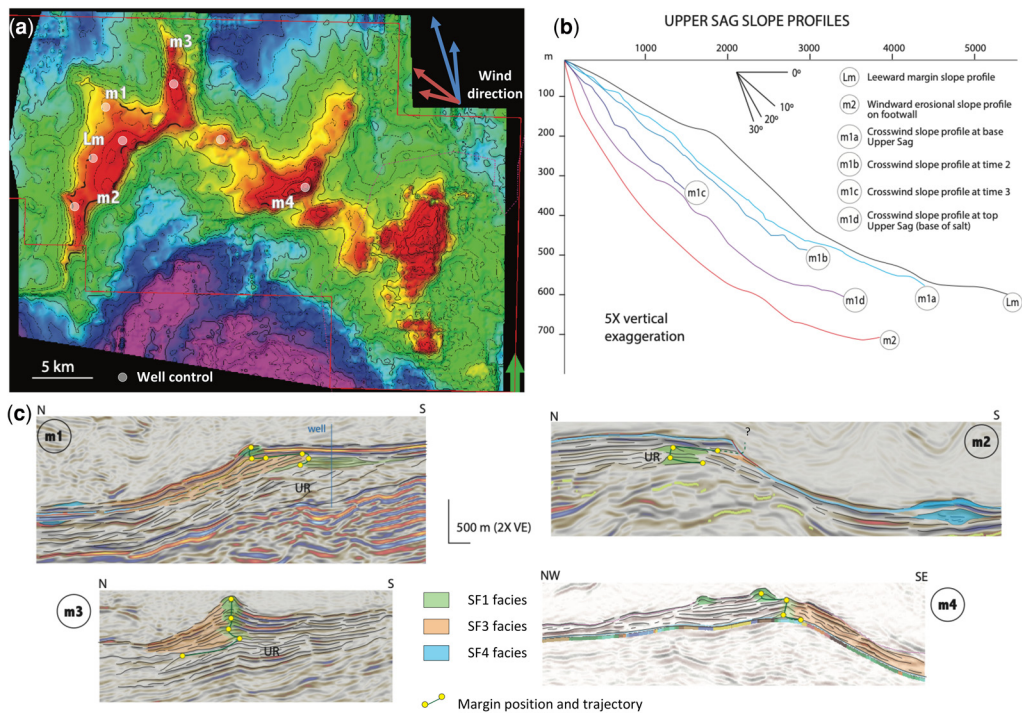


Fig. 12. Margin architecture, stacking pattern, and slope geometry along different areas of the Libra structure. **(a)** Top BVE100 (base salt) structure map of Libra showing three distinct highs. **(b)** Comparison of BVE100 slope profiles along a leeward margin (Lm) and a faulted, windward margin (m2). Slope profiles m1a to m1d show steepening through time at location m1. **(c)** Interpreted seismic lines across the margin and slope in four different areas (see (a) for location). UR, Upper Rift (Itapema and BVE300). Note truncation of platform top SF2 reflectors in m2 and occurrence of SF4 facies (marked in blue) in the adjacent low. Note also that the control well in m1 penetrates parallel and mounded reflectors in the Barra Velha, and inclined reflectors in the UR.

Large indentations up to several kilometres wide along the platform margin fringe all major palaeohighs and are especially well developed along faulted margins abutting deep basins (Figs 2, 5, 12 & 13b). In these areas tabular parallel reflectors (SF2; Table 1) of the platform top are truncated (Fig. 12c) and clinoform angles, where preserved, are steeper than average, with values of approximately 20° and up to more than 30° along the truncation surfaces (erosional margins; Fig. 12). It is noteworthy that no significant progradation is observed along the steepest margins, even outside the arcuate truncation features (Fig. 11a). These features are interpreted as margin collapse scars based on their morphology and size, and truncation of platform top reflectors (Lehrmann *et al.* 2020).

Facies mapping of BV100 over prominent basement highs in the north part of the Santos Basin, such as in Libra and Buzios (Fig. 1), indicates only local progradation and certainly with significantly less lateral expansion (less than 2 km) compared with the underlying Itapema, which locally records

lateral expansion greater than 6 km (Figs 4 & 12c). Where significant progradation did occur, evidence of local progressive steepening of clinoforms is interpreted as *in situ* accretion and early lithification based on analogy with other steepening-outward prograding systems (Fig. 12b; Minzoni *et al.* 2013; Minzoni *et al.* 2017). Extensive occurrence of arcuate truncation surfaces at the platform margin interpreted as collapse features also points to early lithification (Minzoni *et al.* 2017; Lehrmann *et al.* 2020).

Mounded facies (SF1; Table 1) in the Upper Sag interval punctuate the shelf break and are generally less than 2 km long and a few tens of metres thick, considerably smaller than their BVE200 equivalent (cf. Barnett *et al.* 2020). These characteristics suggest filling of accommodation in high-energy settings and potential development of elevated shoals or exposed islands (Minzoni *et al.* 2017). A high-energy shoal complex interpretation is reinforced by the local occurrence of shingled reflectors interpreted as clinoforms within at least some of the SF1 facies and thick accumulations

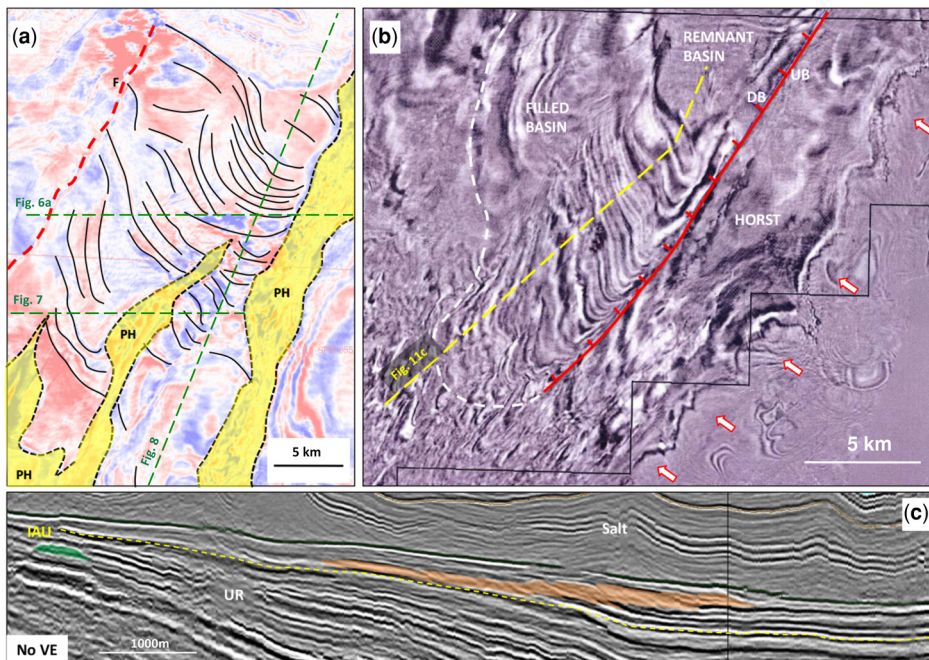


Fig. 13. Amplitude depth slices from near the base-salt reflector (BVE100 interval) showing distinctly arcuate geometry of shelf margin trends within two embayments in the Sugar Loaf High. See Figure 2 for location. (a) Northern end of the Sugar Loaf shelf. PH, Palaeohigh. (b) Northward progradation of intra-shelf clinoforms onto an intra-high remnant basin. Note the arcuate shape of the prograding clinoforms. Arrows point to collapse scars along the SE margin of the Sugar Loaf High. F, Fault; UB, up-thrown block; DB, down-thrown block. (c) Seismic line through the progradation wedge in (b). Prograding clinoforms (facies SF3) are highlighted in orange. Note also local SF1 (mounded) facies in the upper rift highlighted in green. UR, Upper rift; IAU, Intra-Alagoas Unconformity.

of intraclastic grainstone beds described from cores that sampled the Gato do Mato ridge (see Fig. 2 for location).

At Libra, the margin stacking pattern within the Sag interval strongly varies laterally, between the three main sectors that sit on distinct basement blocks, indicating differential subsidence through the structure and impact of initial bathymetry on sequence development (Fig. 12). The mounded facies (SF1; Table 1) are generally very subdued to the west and become progressively thicker and vertically stacked or even backstepped to the east over the central sector, suggesting significantly increased subsidence in that direction (Minzoni *et al.* 2017).

Discussion

Depositional model of presalt carbonate systems and lake palaeobathymetry

The fundamental seismic-scale building block of the presalt carbonate system has a distinct sigmoidal shape (Figs 8 & 10), which records preferential

carbonate sediment accumulation in shallow water over or around palaeohighs, where carbonate units are thicker, and a downward tapering of carbonate production and accumulation with water depth (Fig. 14). The lateral distribution of calibrated seismic facies within the sigmoidal building block indicates that shallow-water accumulation consisted of reworked spherulite or intraclastic grainstone and shrubby boundstone with local occurrence of microbial boundstone along the shelf margins, and spherulite packstone–wackestone in areas protected from currents and waves (Fig. 13). Deposition in deeper water along the slopes consisted of spherulite grainstone to wackestone containing a progressively greater amount of finely laminated shale, which is the dominant lithofacies in basinal or profundal areas, away from the shelf margins (Figs 14 & 15).

The shapes and dimensions of individual clinoforms can be used to empirically evaluate the bathymetry of the presalt lakes at time of carbonate deposition. The height of clinoforms in the Santos Basin varies between roughly 200 m and more than 800 m, with an average of circa 350 m. Erosional

Seismic architecture of lacustrine presalt carbonate systems

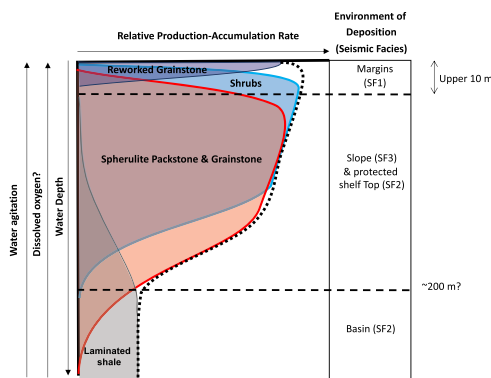


Fig. 14. Interpreted sediment production and accumulation curve for the main Upper Barra Velha carbonate lithofacies. Note the general tapering with increasing water depth (dotted line).

and collapse slopes reach higher values but the measured height values in these types of slope are less reliable as a proxy for palaeobathymetry, because they may have been accentuated by later fault reactivation. Even if not corrected for differential compaction, these values attest that the presalt carbonate sediments were deposited on and around local highs within deep lacustrine basins. The occurrence of collapse features and corresponding chaotic, fan-shaped reflectors at the toe of the slope are interpreted as mass transport deposits (Figs 4a, 5a, 6c, 8b & 12c) along major drop-offs. Perhaps more significantly, the local climbing downlap geometry of BVE100 reflectors onto elevated features of the underlying BVE200 interval corroborates the existence of a rugged topography and deep basins.

During deposition of the BVE100, regional toplap geometries and margin downstepping indicate

that accumulation of carbonate sediment had shifted from the shelf top to the slope. This series of forced regression events (Figs 3 & 6–8), albeit punctuated by minor aggradation of the margins, records significant and progressive shrinkage, partial desiccation of the lakes, and prolonged exposure of the platform tops. Well-preserved inclined reflectors at the base of the salt, however, indicate a final water depth of 150 m or greater, at least locally.

These observations, based on calibrated seismic data, are in stark contrast with the flat and shallow lake model proposed by some workers (Wright and Barnett 2017; Wright and Rodriguez 2018), which is based on core analyses alone and rely upon a geochemical model for the precipitation of Mg-rich clay minerals (stevensite; Tosca and Wright 2015; Wright and Tosca 2016; Wright and Rodriguez 2018). It is noteworthy, however, that the model proposed by Wright and co-authors dismisses the observation of clinoforms as geophysical artefacts or, more baffling, hinges on a regional flattening of the seismic images at the base of salt (top carbonates), and assumes that lacustrine carbonate systems cannot produce thick accumulations of mounded features akin to those observed in marine systems. This assumption, however, is based on our current poorly defined models of lacustrine carbonate settings. Additionally, it should be noted that even when discounting internal prograding reflections within the Barra Velha as geophysical artefacts, the overall draping geometry of the BVE100-BVE200 would still imply significant bathymetry at the time of deposition. Furthermore, the Cretaceous presalt lakes differ greatly from both modern and ancient lacustrine analogues in terms of texture and thickness of carbonate deposits, water chemistry and size. Large and deep presalt lakes could have generated enough fetch, tides and storms to be more similar to ocean basins than our current lacustrine models

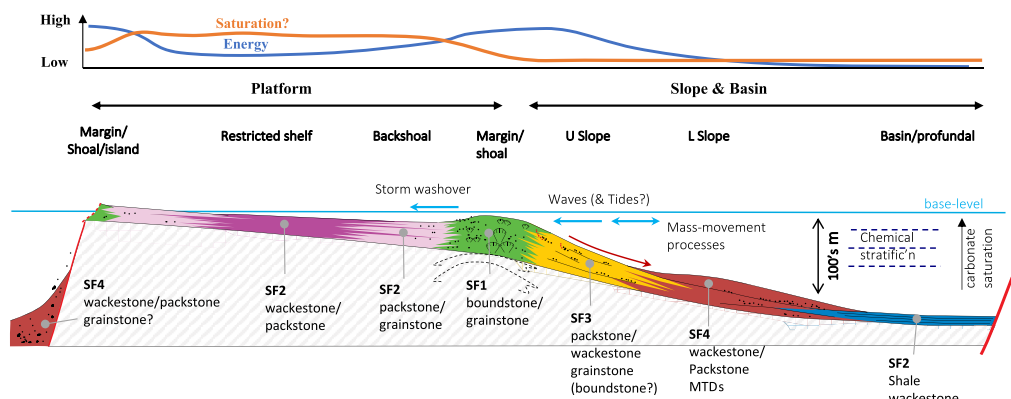


Fig. 15. Schematic depositional model for the Upper Barra Velha interval and correlative seismic facies and lithofacies. MTDs, mass transport deposits.

predict. Perhaps a strong chemical stratification in the presalt lake waters could be invoked to explain both the abundant precipitation of Mg-rich clays such as stevensite and the occurrence of deep water.

The local occurrence of clinoforms within the upper rift section supports a similar depositional model for the coquina (Itapema Formation). Mounded facies (SF1; **Table 1**) within the Itapema interval are relatively extensive and rooted onto the underlying topographic highs. They are interpreted as the production *loci* of the shell material that was either locally reworked into shoals or transported downslope to form prograding clinoform packages. Despite the apparent lack of boundstone in the Itapema, these clinoforms are comparable in size and dip angle with those observed in the Barra Velha (**Fig. 4**; Barnett *et al.* 2020). Steep slopes may have resulted from deposition of the coarse shell material at angle of repose, early cementation and stabilization of slope sediment, or both. The occurrence of large collapse and healed scars along the margins of Libra (**Fig. 4**) suggests that early cementation may have played a role, at least locally. It is also important to note that progradation of the Itapema did not fill the basin and that the youngest clinoforms attained at least 350 m in height (**Fig. 4**), recording a very steep and rugged palaeotopography at time of initial deposition of the Barra Velha. A switch to shallow lakes across the PAU would not only imply a lake level drop of >350 m, but also a very prolonged exposure of the top and slope of the Itapema interval.

Controls on sequence-stratigraphic architecture

In marine settings the large-scale architecture of carbonate systems is controlled in first principle by the antecedent topography, the available accommodation and its lateral and vertical variation through time (tectonic setting) and the carbonate factory type (e.g. Pomar 2001; Bosence 2005; Schlager 2005; Dorobek 2008; Minzoni *et al.* 2013). The same first-order controls must operate in any type of sedimentary basin, including lacustrine systems, as long as there is sufficient supersaturation and precipitation of calcium carbonate, either biotically or abiotically. The main difference between lacustrine and marine systems of comparable size is the water chemistry and therefore the carbonate factory type (Minzoni *et al.* 2017; Eberli *et al.* 2019). Large lacustrine systems characterized by tapering saturation with water depth would therefore mimic marine systems, except for the details of the carbonate components and perhaps the high-frequency stratigraphic architecture.

The stacking pattern of sigmoidal building blocks mapped in the presalt unit records the complex

sequence stratigraphic architecture of lacustrine carbonate systems. The position of the shelf margin through time in prograding intervals of the BVE100 can be confidently correlated only locally, within major basement highs, suggesting that the lakes may have become locally isolated during times of lake-level fall and lowstand, rather than being a single continuous lake. By the same token, regional correlation of carbonate strata on depositional highs and intervening lows during the highstand periods indicates that the highstand lakes were deep, very continuous and probably areally comparable to oceanic basins.

The stacking pattern of mounded marginal facies (SF1; **Table 1**) across the IAU boundary shows the impact of subsidence and accommodation on architectural style (**Figs 3, 6 & 8**). Relatively rapid but laterally variable subsidence across rotating normal fault blocks produced aggradational and local backstepping of the marginal mounds in the Lower Barra Velha BVE300 interval. Reduced subsidence rates during thermal isostatic re-equilibration allowed significant progradation of the shelf margin in the Upper Barra Velha interval. Lateral variation in accommodation via differential subsidence at Libra resulted in varying stacking patterns, from progradation in the NW sector to aggradation and backstepping in the central sector (**Fig. 12**).

Large-scale base-level variations recorded by vertical shifting of the margin of up to 200 m are the probable driver of higher-order sequences observed in the BVE100 interval (**Figs 6–8**). Similar variations may have occurred in the BVE200 and BVE300 as well, but the dominant aggradational pattern typical of these intervals makes it more difficult to resolve high-order sequences owing to the vertical stacking of the seismic facies.

The antecedent topography inherited from multi-phase rifting of the basement exerted an additional major control on the architecture and facies distribution in the presalt carbonate systems. Shallow basinal areas with limited accommodation are associated with greater progradation of generally gentler slopes and coalescence of smaller nuclei into larger megaplatforms (Minzoni *et al.* 2017; Simo *et al.* 2019). Faulted highs abutting deeper basinal areas and basement drop-offs in excess of 500 m are associated with lesser progradation, steeper slope angles and, in extreme cases, aggradation of fringing boundstone or grainstone mounds (**Fig. 11a**) and margin failure by sector collapse (**Figs 5a, 7b & 12c**). A clear example is recorded in the Sugar Loaf High, where carbonate strata of the Barra Velha deposited at the margins of a high-relief horst structure exhibit an aggradational pattern, with local backstepping (**Fig. 7**).

Erosion and collapse of high-relief margins is particularly well expressed along the high-relief (>1000 m), steep ($>30^\circ$) southeastern boundary of

Seismic architecture of lacustrine presalt carbonate systems

both the Sugar Loaf High and the Tupi High (Figs 7b & 11a), where large collapse scars, 3–5 km wide, caused deep erosion of the carbonate margin (Buckley *et al.* 2015; Minzoni *et al.* 2017; Figs 2 & 13b). Time-equivalent strata deposited in significantly shallower water (generally only up to 350 m) along the margins of internal basins perched on the main structural highs are characterized by strongly prograding reflectors (Figs 6–9 & 13c; Tremblay *et al.* 2014; Buckley *et al.* 2015; Minzoni *et al.* 2017). Similarly, progradation was more pronounced where basin infill occurred, which effectively decreased water depth and thus the relief of the carbonate margin. This is particularly evident in the area between the Sugar Loaf High and the Tupi High, where thick, basinal accumulation of volcanic rocks and volcanoclastic strata of the BVE300 was associated with later (Upper Barra Velha) progradation of the shelf margin (Figs 3 & 8).

Sediment accumulation at the toe of slope also affected the geometry of the prograding clinoforms. Prograding reflectors over starved basinal areas are typically tabular, with steep, linear slopes (Fig. 10b), while prograding reflections over areas of thick basinal accumulation display a characteristic climbing and flattening outward geometry (Bosellini 1984), and have a distinct exponential shape with tangential lower slope (Adams and Kenter 2013; Figs 6, 7a & 10a).

Palaeowind direction and surface currents had a significant impact on facies distribution and large-scale geometries as inferred from consistent asymmetries interpreted as windward–leeward effects (Fig. 9). Palaeoclimatic models indicate southerly to southeasterly trade winds, resulting in windward margins facing south and SE and leeward, progradational margins facing north and NW. The complex topography, however, may have affected significantly the current direction, at least locally. Sheltered versus open circulation could also result from the presence or absence, respectively, of persistently exposed features such as islands (Fig. 11), or simply by slight variations in water depth at the lake floor. The presence of islands along the southeastern margin of the Tupi High is confirmed by onlapping of top Barra Velha reflectors on both sides of the palaeohigh (Fig. 11a). Wells that penetrated the sheltered, vast and shallow area leeward (west) of the island encountered a significantly greater proportion of fine-grained, microporous, Mg-clay-rich lithologies than the few that tested the windward side (east) of the island, where sheltering was not effective (Fig. 11). Removal of the Mg-clay, however, may have also occurred diagenetically, at least in part (Tosca and Wright 2015; Wright and Barnett 2015; Wright and Rodriguez 2018).

The concave arcuate geometry in plan-view of prograding clinoforms within embayments

(Fig. 13) suggests that significant lateral transport of carbonate particles by drift currents may have occurred (Tremblay *et al.* 2014; Minzoni *et al.* 2017). Arcuate accretion of beach ridges is reported from coastal marine environments as well as large lakes. Lake Michigan accumulated up to 5 km of arcuate strand plain sediments in 3000 years (Thompson and Baedke 1997). Although the arcuate prograding wedges in the Upper Barra Velha interval are similar in geometry and shape to the ones described from modern lakes, the vertical dimension of the clinoforms (up to 300 m) is much larger in the presalt section, attesting to significantly deeper lakes and perhaps stronger storm activity.

Conclusions

Despite their peculiar petrographic and textural composition, the presalt lacustrine carbonate intervals of the Santos Basin show all of the salient large-scale sequence-stratigraphic characteristics known and described from marine carbonate systems developed in both active and passive tectonic settings.

Synrift and post-rift carbonate systems in the Santos Basin are characterized by complex stratigraphy. The large-scale architecture as interpreted from calibrated seismic data was controlled primarily by subsidence patterns, antecedent topography and the production curve of the carbonate factory. The spatial and temporal accumulation pattern of basinal siliciclastic and volcanic strata contributed to the determination of progradation versus aggradation geometries and controlled the shape of the slope by modifying the platform relief. High-amplitude base-level fluctuations modified but did not dramatically alter the basic architectural evolution of the carbonate systems.

Shelf margins aggraded and backstepped during rifting atop horst structures or tilted basement blocks, where asymmetric evolution of the platform resulted from active rotation of the underlying basement. The depositional architecture of carbonate margins off the structural highs during the sag phase, when thermal, post-rift subsidence prevailed, is strongly progradational to downstepping, reflecting lower subsidence rates and perhaps increased production rates. Widespread downstepping in the Upper Barra Velha suggests exposure, and possibly erosion, of the shelf top prior to deposition of the salt.

The sigmoidal geometry of the individual sequences indicates a tapering production with water depth, similar to that described from marine analogues. The steepness and size of inclined reflections, interpreted as slope deposits, imply that water depth was significant, up to several hundred metres, and the occurrence of arcuate strand plain beach

ridges suggests that storms and possibly deep-water currents exerted an important role in sediment reworking and accumulation. In contrast to previous core-based depositional models advocating a shallow and flat lake bottom bathymetry, evidence from calibrated seismic data indicates that the presalt lakes were deep and wide, at least episodically, and that the distribution of depositional facies both laterally and along the shelf profile was controlled by energy of the environment, regardless of the specific type of carbonate producer.

This study shows that predicting reservoir quality distribution in the presalt carbonate play and analogue systems requires process-based conceptual models incorporating a detailed understanding of the factors controlling the sequence stratigraphic architecture and lateral facies distribution.

Acknowledgments We wish to thank the Shell Pre-Salt Brasil Growth Team, Shell Specialized Geology Team (Netherlands) and Brasil Subsurface Technology for extensive collaboration and technical support. Interpretation was carried out under the auspices of Fred Keller, Gary Steffens, Peter Winefield, Jurriaan Reijns, Lucio Prevattti, Joris Grimbergen, Vanessa Kertznus, Barnaby Philips and Gabriel Guerra (Shell). We also thank the Libra JV composed by PETROBRAS, CNPC, CNOOC Limited, TOTAL, Shell Brasil Petróleo and Pré-Sal Petróleo SA (PPSA) as manager of the Production Sharing Agreement for allowing the publication. Particular thanks to Rudolf Van Den Oord from Front End Development team in Shell. We thank CGG Veritas for permission to publish their seismic data; all seismic images are from the CGG PSDM Cluster 3D volume and Libra. We are grateful to Volume Editor David Hunt, Coordinating Editor James Hendry and two anonymous reviewers for their insightful comments and edits that improved the manuscript.

Author contributions **MM:** conceptualization (lead), data curation (equal), formal analysis (lead), investigation (lead), methodology (lead), project administration (equal), supervision (equal), validation (lead), visualization (lead), writing – original draft (lead), writing – review & editing (lead); **AC:** conceptualization (equal), data curation (equal), formal analysis (equal), investigation (equal), methodology (equal), project administration (equal), validation (equal); **JT:** data curation (supporting), formal analysis (supporting), investigation (supporting); **BW:** conceptualization (supporting), project administration (equal), resources (equal), supervision (supporting), writing – review & editing (supporting).

Funding This research received no specific grant from any funding agency in the public, commercial, or not-for-profit sectors.

Data availability The datasets analysed during the current study are not publicly available due to their proprietary nature.

References

- Adams, E.W. and Kenter, J.A.M. 2013. So diferente, yet so similar: comparing and contrasting siliciclastic and carbonate slopes. *In: Verwer, K., Playton, T.E. and Harris, P.M. (eds) Deposits, Architecture and Controls of Carbonate Margin, Slope and Basinal Settings. SEPM Special Publications*, **105**, 14–25.
- Arienti, L.M., Souza, R.S. *et al.* 2018. Facies association, depositional systems, and paleophysiographic models of the Barra Velha Formation, Pre-Salt Sequence – Santos Basin, Brazil. *AAPG Search and Discovery*, article no. 90323.
- Bachtel, S.L., Kissling, R.D., Martono, D., Rahardjanto, S.P., Dunn, P.A. and MacDonald, B.A. 2004. Seismic stratigraphic evolution of the Miocene Pliocene Segitiga Platform, East Natuna Sea, Indonesia: the origin, growth, and demise of an isolated carbonate platform. *In: Eberli, G.P., Masaferro, J.L. and Sarg, J.F. (eds) Seismic Imaging of Carbonate Reservoirs and Systems. AAPG Memoirs*, **81**, 309–328.
- Barnett, A.J., Fu, L., Rapasi, T., Scotellaro, C., Guha, J., Cabolova, A. and Domingues, A.L. 2020. Seismic characterisation and origin of clinoforms in lacustrine depositional environments: a case study from the Cretaceous of the South Atlantic. *Geological Society, London, Special Publications*, **509**.
- Bastianini, L., Rogerson, M., Mercedes-Martín, R., Prior, T.J., Cesar, E.A. and Mayes, W.M. 2019. What causes carbonates to form 'shrubby' morphologies? An Anthropocene limestone case study. *Frontiers in Earth Sciences*, **7**, 1–19, <https://doi.org/10.3389/feart.2019.00236>.
- Bosellini, A. 1984. Progradation geometries of carbonate platforms: examples from the Triassic of the Dolomites, northern Italy. *Sedimentology*, **31**, 1–24, <https://doi.org/10.1111/j.1365-3091.1984.tb00720.x>.
- Bosence, D.W.J. 2005. A genetic classification of carbonate platforms based on their basinal and tectonic settings in the Cenozoic. *Sedimentary Geology*, **175**, 49–72, <https://doi.org/10.1016/j.sedgeo.2004.12.030>.
- Buckley, J.P., Bosence, D.W.J. and Elders, C. 2015. Tectonic setting and stratigraphic architecture of an Early Cretaceous lacustrine carbonate platform, Sugar Loaf High, Santos Basin, Brazil. *Geological Society, London, Special Publications*, **418**, 175–191, <https://doi.org/10.1144/SP418.13>.
- Carminatti, M., Wolff, B. and Gamboa, L.A.P. 2008. New exploratory frontiers in Brazil. *19th World Petroleum Congress*, Madrid, 29 June to 3 July 2008.
- Carminatti, M., Dias, J.L. and Wolff, B. 2009. From turbidites to carbonates: breaking paradigms in deep waters. *Offshore Technology Conference*, Houston, Texas, 2012.
- Catuneanu, O., Abreu, V. *et al.* 2009. Towards the standardization of sequence stratigraphy. *Earth Science Review*, **92**, 1–33, <https://doi.org/10.1016/j.earscirev.2008.10.003>.
- Ceraldi, T.S. and Green, D. 2017. Evolution of the South Atlantic lacustrine deposits in response to Early Cretaceous rifting, subsidence and lake hydrology. *Geological Society, London, Special Publications*, **438**, 77–98, <https://doi.org/10.1144/SP438.10>.
- Davison, I. 2007. Geology and tectonics of the south Atlantic Brazilian salt basins. *Geological Society, London*,

Seismic architecture of lacustrine presalt carbonate systems

- Special Publications*, **272**, 345–359, <https://doi.org/10.1144/GSL.SP.2007.272.01.18>
- Della Porta, G. 2015. Carbonate build-ups in lacustrine, hydrothermal and fluvial settings: comparing depositional geometry, fabric types and geochemical signature. *Geological Society, London, Special Publications*, **418**, 17–68, <https://doi.org/10.1144/SP418.4>
- Della Porta, G., Merino-Tome, O., Kenter, J.A.M. and Verwer, K. 2013. Lower Jurassic microbial and skeletal carbonate factories and platform geometry (Djebel Bou Dahir, High Atles, Morocco). In: Verwer, K., Playton, T.E. and Harris, P.M. (eds) *Deposits, Architecture and Controls of Carbonate Margin, Slope and Basinal Settings*. SEPM Special Publications, **105**, 237–263.
- De Luca, P., Carballo, J., Filgueiras, A., Pimentel, G., Esteban, M., Tritlla, J. and Villacorta, R. 2015. What is the role of volcanic rocks in the Brazilian Pre-Salt? (Extended abstracts.) *77th EAGE Conference & Exhibition, IFEMA*, Madrid, Spain, 1–4 June 2015, <https://doi.org/10.3997/2214-4609.201412890>
- Dias, J.L. 2005. Tectônica, estratigrafia e sedimentação no Andar Aptiano da margem leste brasileira. *Boletim de Geociências da Petrobrás*, **13**, 7–25.
- Dorobek, S.L. 2008. Tectonic and depositional controls on syn-rift carbonate platform sedimentation. In: Lukasik, J.A. and Simo, J.A. (Toni) (eds) *Controls on Carbonate Platform and Reef Development*. SEPM Special Publications, **89**, 57–81.
- Eberli, G.P. and Ginsburg, R.N. 1987. Segmentation and coalescence of Cenozoic carbonate platforms, northwestern Great Bahama Bank. *Geology*, **15**, 75–79, [https://doi.org/10.1130/0091-7613\(1987\)15<75:SA COCC>2.0.CO;2](https://doi.org/10.1130/0091-7613(1987)15<75:SA COCC>2.0.CO;2)
- Eberli, G.P., Sousaari, E., Karaca, E., Diaz, M., Betzler, C. and Ludmann, T. 2019. Lessons from Hamelin Pool and the Maldives for the coquina reservoir in Libra, Santos Basin. (Abstracts.) *AAPG Annual Meeting (ACE)*, San Antonio, TX.
- Fairhead, J.D. and Wilson, W. 2005. Plate tectonic processes in the South Atlantic Ocean: do we need deep mantle plumes? In: Fougner, G.R., Natland, J.H., Prentiss, D.C. and Anderson, D.L. (eds) *Plate, Plumes, and Paradigms*. Geological Society of America, Special Papers, **388**, 537–553.
- Galloway, W.E. 1989. Genetic stratigraphic sequences in basin analysis 1: architecture and genesis of flooding-surface-bounded depositional units. *AAPG Bulletin*, **73**, 125–142.
- Goodfriend, G.A. and Stanley, D.J. 1999. Rapid strandplain accretion in the northeastern Nile delta in the 9th century A.D. and the demise of the port of Pelusium. *Geology*, **27**, 147–150.
- Guardado, L.R., Gamboa, L.A.P. and Lucchesi, C.F. 1990. Petroleum geology of the Campos Basin, Brazil: a model for producing Atlantic-type basins. In: Edwards, J.D. and Santogrossi, P.A. (eds) *Divergent-passive margin basins*. American Association of Petroleum Geologists, Memoirs, **48**, 3–80.
- Kattah, S. 2017. Exploration opportunities in the Pre-Salt play, Deepwater Campos Basin, Brazil. *The Sedimentary Record*, **15**, 4–8, <https://doi.org/10.2110/sedred.2017.1.4>
- Lehrmann, D.J., Minzoni, M. et al. 2020. Giant sector-collapse structures (scalloped margins) of the Yangtze Platform and Great Bank of Guizhou, China: implications for genesis of collapsed carbonate platform margin systems. *Sedimentology*, **67**, <https://doi.org/10.1111/sed.12740>
- Liechoscki de Paula Faria, D., Tadeu dos Reis, A. and Gomes de Souza, O., Jr. 2017. Three-dimensional stratigraphic-sedimentological forward modelling of an Aptian carbonate reservoir deposited during the sag stage in the Santos basin, Brazil. *Marine and Petroleum Geology*, **88**, 676–695, <https://doi.org/10.1016/j.marpetgeo.2017.09.013>
- Lomask, J., Francis, J.M., Rickett, J., Buursink, M.L., Gerber, T.P., Perlmutter, M. and Paola, C. 2009. New tools for seismic stratigraphic interpretation: stratal convergence and instantaneous isochron attribute cubes derived from volumetric flattening of experimental strata. *AAPG Bulletin*, **93**, 453–459, <https://doi.org/10.1306/11200808104>
- Mello, M.R., Macedo, J.M., Requejo, R. and Schiefelbein, C. 2002. The Great Campos: a frontier for new giant hydrocarbon accumulations in the Brazilian sedimentary basins. (Abstract.) *AAPG Bulletin*, **85**, 13, <https://doi.org/10.1306/61EEC78E-173E-11D7-8645000102C1865D>
- Mercedes-Martín, R., Brasier, A.T., Rogerson, M., Reijmer, J.J.G., Vonhof, H. and Pedley, M. 2017. A depositional model for spherulitic carbonates associated with alkaline, volcanic lakes. *Marine and Petroleum Geology*, **86**, 168–191, <https://doi.org/10.1016/j.marpetgeo.2017.05.032>
- Mercedes-Martín, R., Ayora, C., Tritlla, J. and Sanchez-Roman, M. 2019. The hydrochemical evolution of alkaline volcanic lakes: a model to understand the South Atlantic pre-salt mineral assemblages. *Earth-Science Reviews*, **198**, 1–19, <https://doi.org/10.1016/j.earscirev.2019.102938>
- Minzoni, M., Lehrmann, D.J. et al. 2013. Triassic tank: platform margin and slope architecture in space and time, Nanpanjiang Basin, south China. In: Verwer, K., Playton, T.E. and Harris, P.M. (eds) *Deposits, Architecture and Controls of Carbonate Margin, Slope and Basinal Settings*. SEPM Special Publications, **105**, 84–113.
- Minzoni, M., Cantelli, A. and Thornton, J. 2017. Seismic-scale geometries and sequence-stratigraphic architecture of Early Cretaceous sun-post rift lacustrine carbonate systems, pre-salt section, South Atlantic margins. In: Hart, B., Rosen, N.C., West, D., D'Agostino, A., Messina, C., Hoffman, M. and Wild, R. (eds) *Sequence Stratigraphy: The Future Defined*. SEPM Gulf Coast Section Publications, <https://doi.org/10.5724/gcs.17.193>
- Mitchum, R.M., Jr. and Van Wagoner, J.C. 1991. High-frequency sequences and their stacking patterns: sequence-stratigraphic evidence of high-frequency eustatic cycles. *Sedimentary Geology*, **70**, 131–160, [https://doi.org/10.1016/0037-0738\(91\)90139-5](https://doi.org/10.1016/0037-0738(91)90139-5)
- Mitchum, R.M., Jr., Vail, P.R. and Sangree, J.B. 1977. Seismic stratigraphy and global change of sea level, part 6: stratigraphic interpretation of seismic reflection patterns in depositional sequences. In: Payton, C.E. (ed.) *Seismic Stratigraphy – Application to Hydrocarbon Exploration*. American Association of Petroleum Geologists, Memoirs, **26**, 117–133.

- Moreira, J.L.P., Valdetaro Madeira, C.V., Gil, J.A. and Machado, M.A.P. 2007. Bacia de Santos. *Boletim de Geociências da Petrobras*, **15**, 531–549.
- Muniz, M.C. and Bosence, D.W. 2015. Pre-salt microbialites from the Campos Basin (offshore Brazil): image log facies, facies model and cyclicity in lacustrine carbonates. *Geological Society, London, Special Publications*, **418**, 221–242, <https://doi.org/10.1144/SP418.10>
- Pereira, M.J. and Feijó, F.J. 1994. Bacia de Santos. Estratigrafia das Bacias Sedimentares do Brasil. *Boletim de Geociências da Petrobrás*, **8**, 219–234.
- Pietzsch, R., Oliveira, D.M. *et al.* 2018. Palaeohydrology of the Lower Cretaceous pre-salt lacustrine system, from rift to post-rift phase, Santos Basin, Brazil. *Palaeogeography, Palaeoclimatology, Palaeoecology*, **507**, 60–80, <https://doi.org/10.1016/j.palaeo.2018.06.043>
- Playton, T.E., Janson, X. and Kerans, C. 2010. Carbonate slopes. *Facies Models*, **4**, 449–476.
- Pomar, L. 2001. Types of carbonate platforms: a genetic approach. *Basin Research*, **13**, 313–334, <https://doi.org/10.1046/j.0950-091x.2001.00152.x>
- Rezende, M.F. and Pope, M.C. 2015. Importance of depositional texture in pore characterization of subsalt microbialite carbonates, offshore Brazil. *Geological Society, London, Special Publications*, **418**, 193–207, <https://doi.org/10.1144/SP418.2>
- Saller, A., Rushton, S., Buambua, L., Inman, K., McNeil, R. and Dickson, J.T. 2016. Presalt stratigraphy and depositional systems in the Kwanza Basin, offshore Angola. *AAPG Bulletin*, **100**, 1135–1164, <https://doi.org/10.1306/02111615216>
- Schlager, W. 1989. Drowning unconformities on carbonate platforms. In: Crevello, P.D., Sarg, J.F., Read, J.F. and Wilson, J.L. (eds) *Controls on Carbonate Platform to Basin Development*. SEPM Special Publications, **44**, 15–25.
- Schlager, W. 2005. Carbonate sedimentology and sequence stratigraphy. *SEPM Special Publications*, **8**, <https://doi.org/10.2110/csp.05.08>
- Simo, T., Sitgreaves, J., Smith, E., Bayram, U. and Stewart, J. 2019. Styles of pre-salt carbonate platforms, Brazil Santos Basin. *AAPG Search and Discovery*, article no. 90350.
- Souza, R.S., Arienti, L.M. *et al.* 2018. Petrology of the hydrothermal and evaporitic continental Cretaceous (Aptian) pre-salt carbonates and associated rocks, South Atlantic Santos Basin, offshore Brazil. (Abstract.) *AAPG Search and Discovery*, article no. 90323.
- Thompson, T.A. and Baedke, S.J. 1997. Strand-plain evidence for late Holocene lake-level variations in Lake Michigan. *Geological Society of America, Bulletin*, **109**, 666–682, [https://doi.org/10.1130/0016-7606\(1997\)109<0666:SPEFLH>2.3.CO;2](https://doi.org/10.1130/0016-7606(1997)109<0666:SPEFLH>2.3.CO;2)
- Tosca, N.J. and Wright, V.P. 2015. Diagenetic pathways linked to labile Mg-clays in lacustrine carbonate reservoirs: a model for the origin of secondary porosity in the Cretaceous pre-salt Barra Velha Formation, offshore Brazil. *Geological Society, London, Special Publications*, **435**, 36–46, <https://doi.org/10.1144/SP435.1>
- Tremblay, S., Verwer, K. and Lukasik, J. 2014. New insight into the seismic architecture of the pre-salt upper sag carbonate depositional system, Brazil. (Abstract.) *AAPG Search and Discovery*, article no. 90189.
- Vail, P.R. 1987. Seismic stratigraphy interpretation using sequence stratigraphy. Part 1: seismic stratigraphy interpretation procedure. In: Balley, A.W. (ed.) *Atlas of Seismic Stratigraphy*. American Association of Petroleum Geologists, Studies in Geology, **27**, 1–10.
- Van Hoek, T., Gesbert, S. and Pickens, J. 2010. Geometric attributes for seismic stratigraphic interpretation. *The Leading Edge*, **29**, 1056–1065, <https://doi.org/10.1190/1.3485766>
- Winter, W.R., Jahnert, R.J. and França, A.B. 2007. Bacia de Campos. *Boletim de Geociências da Petrobras*, **15**, 511–529.
- Wright, V.P. 2010 Reservoir architectures in non-marine carbonates (abs.). AAPG Annual Convention and Exhibition, 10–13 April, Houston, Texas, USA. Search and Discovery Article #40801.
- Wright, V.P. 2012. Lacustrine carbonates in rift settings: the interaction of volcanic and microbial processes on carbonate deposition. *Geological Society, London, Special Publications*, **370**, 39–47, <https://doi.org/10.1144/SP370.2>
- Wright, V.P. and Barnett, A.J. 2015. An abiotic model for the development of textures in some South Atlantic early Cretaceous lacustrine carbonates. *Geological Society, London, Special Publications*, **418**, 209–219, <https://doi.org/10.1144/SP418.3>
- Wright, V.P. and Barnett, A.J. 2017. Critically evaluating the current depositional models for the pre-salt Barra Velha Formation, offshore Brazil. (Abstract.) *AAPG Search and Discovery*, article no. 51439(2017).
- Wright, V.P. and Rodriguez, K. 2018. Reinterpreting the South Atlantic pre-salt ‘microbialite’ reservoirs: petrographic, isotopic and seismic evidence for a shallow evaporitic lake depositional model. *First Break*, **36**, 71–77.
- Wright, V.P. and Tosca, N.J. 2016. A geochemical model for the formation of the pre-salt reservoirs, Santos Basin, Brazil: implications for understanding reservoir distribution. *AAPG Search and Discovery*, article no. 51304.